Mitigation of Acoustic Noise and Vibration in Permanent Magnet Synchronous Machines Drive using Field Reconstruction Method

B. Sutthiphornsombat, A. Khoobroo, B. Fahimi, *Senior Member, IEEE*

***Abstract*- Due to high torque-to-loss ratio, permanent magnet synchronous machines (PMSM) have received increasing attention in automotive applications. In addition to high efficiency, quiet operation of the propulsion drives are desirable in automotive, naval and military applications. To effectively mitigate the effects of acoustics noise and vibration in PMSM, a numerically efficient method for optimization is necessary. Field reconstruction method (FRM) is presented and used to mitigate the acoustic noise and vibration in PMSM drives. To accomplish this goal, the three-phase current and rotor position of PMSM were used in the FRM computation. The experimental results show that FRM can effectively mitigate the acoustic noise and vibration caused by the PMSM. Our investigations indicate that FRM can precisely calculate the torque pulsation.**

I. INTRODUCTION

High power density, absence of brushes, high torque/inertia ratio, and negligible rotor losses make permanent magnet synchronous machines (PMSM) a competitive candidate for many, high-performance, and servo applications including those used in vehicular industry. High level of tangential and radial vibrations in PMSM drives have been reported by several researchers over the past decades [1]-[5]. In order to remedy these undesirable effects several methods have been proposed on how to numerically calculate the electromagnetic forces in PMSM. While the radial vibration of the stator frame is partially responsible for undesirable acoustic noise, pulsation in electromagnetic torque can escalate undesirable vibrations and potential damages to the components that are in tandem with the motor shaft. This in turn can reduce the effective lifetime of the motor and other mechanical components in the power train.

Once radial and tangential forces acting on the rotor and stator of a PMSM drive are calculated an optimization method can be employed to minimize the pulsation which leads to reduction of the acoustic noise and vibration originated from radial/tangential forces acting on the structure of the PMSM [2]. Notably the most considerable computation is on how to accurately compute torque and radial force pulsations.

Vibration in electric machines can be classified into two major categories namely, tangential and radial. While radial vibration causes vibration of the motor frame in radial direction, the tangential vibration generates pulsations acting on the shaft and therefore components that are in tandem with the shaft. Torque pulsation in PMSM can be attributed to numbers of sources, including the structure design of the machine, unbalanced operation, non-sinusoidal distribution of the magneto-motive force, and error in feedback measurement and controls. The tangential force is dependent upon the distribution of the magnetic field in the air gap. One of the methods that are employed to analyze torque pulsation is based on finite element analysis (FEA). Nevertheless, in practice FEA is not suitable for the real time torque ripple minimization because of its relatively long computational time[3]-[4].

Field reconstruction method (FRM) is proposed to compute the electromagnetic torque and radial forces of PMSM in this paper. The FRM utilizes the three phase current profile and rotor position to calculate radial and tangential components of the force density and the flux density as shown in Fig 1. Furthermore, FRM can predict torque ripple originated from geometry of the machine. Stator slots play a central role in the profile of the torque ripple when there is no stator excitation (i.e. cogging torque).

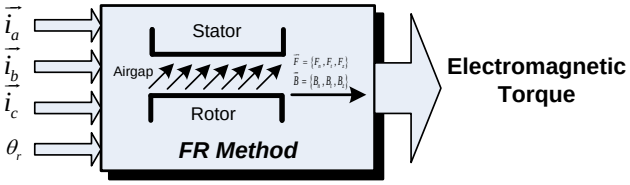

Fig. 1: Block diagram of field reconstruction method

II. FIELD RECONSTRUCTION METHOD

1. *Force and torque distribution in PMSM*

The acoustic noise and vibration in PMSM are caused by the electromagnetic tangential and radial forces. While radial vibration causes vibration of the motor frame in radial direction, the tangential vibration generates pulsations acting on the shaft (and components that are in tandem with the shaft).

A. Radial forces

Radial forces are usually viewed as the unwanted byproduct of electromechanical energy conversion process. Due to the fact that these forces act in a direction perpendicular to that of the rotary motion, their contribution to the motional torque is non-existent. However, they can potentially contribute to significant vibration in the stator frame. It must be noted that the spatial distribution of radial forces on the surface of the stator tooth results in a rather complex structural behavior. To

the contrary, the tangential component of the electromagnetic forces contribute to the motional forces by a great extent. Using Maxwell stress method distribution of the radial and tangential force densities in the airgap of the machine is given by:

$$f_n = \frac{1}{2\mu_0}(B_n^2 - B_t^2) \quad (1)$$

$$f_t = \frac{1}{\mu_0}(B_n B_t) \quad (2)$$

where f_n, f_t, B_n, B_t and μ_0 denote the normal component of the force density, the tangential component of the force density, the normal component of the flux density, the tangential component of the flux density and absolute permeability, respectively.

B. Tangential forces

The electromagnetic torque of PMSM is generated by the virtue of the tangential forces acting on the rotor. However, the tangential forces that are produced on the surface of stator poles will cause unwanted tangential vibrations in the stator frame. Therefore, mitigation of acoustic noise and vibration in the stator includes not only the normal, but also the tangential forces.

The magnetic field density and magnetic energy inside the unsaturated ferromagnetic material are very small. Therefore, the force contribution from these components are expected to be very small.

Radial forces throughout any component exhibit different magnitudes at different locations. Therefore, compensation cannot always be based on the average values measured in the machine and local effects need to be taken into account. In addition, local saturation is observed at pole tips owing to a large concentration of magnetic flux. This causes a much larger force at the tip of the stator poles than the rest of the pole. At the surface of a material with high permeability, the tangential component of flux density is almost equal to zero, and the normal force density almost entirely depends on normal component of flux density.

Finally, from an energy point of view, almost all the energy exchange happens at the iron-air interface as the system moves [3]. In fact, a region with highest energy density is replaced by a region with almost zero energy density. As a result the highest rate of energy exchange within an incremental displacement happens at the interface of iron and air, thus almost the majority of all forces on the interface constitute normal component toward the air.

2. Field reconstruction method (FRM)

In the electromechanical energy conversion (EMEC), it is very important to obtain the flux density distribution. This is the key observation in development of the field reconstruction method (FRM). As seen in Fig.1, FRM requires the input of three-phase current profiles and rotor position to calculate the flux density distribution.

In order to efficiently develop a FRM model of the machine, a series of snapshots from the magnetic field distribution in the targeted area is necessary. In this study the finite element analysis (FEA) is utilized to collect these snapshots. To accomplish this goal, the commercially available software- Magnet® by Infolytica was used. For a complete simulation of the 3-phase permanent magnet synchronous machine, there are four basic inputs. They include three phase currents and the angular position of the rotor. The resultant normal and tangential components of flux density in the airgap for any rotor position were obtained using a few snapshots of the magnetic field distribution. Corresponding force densities were calculated using Maxwell Stress Tensor method as described in equations (1) and (2).

A field reconstruction method (FRM) is proposed to compute the electromagnetic torque and radial forces of PMSM. The FRM utilizes the three phase current profile and rotor position to calculate radial and tangential components of the force density and the flux density. As can be noted from Fig.1, using an appropriate integration contour around the stator and rotor, the actual force acting on each surface can be computed by integrating the force density components over the respective surface area as follows:

$$F_t = \oint_S \vec{f}_t dS \quad (3)$$

$$F_n = l \int_0^{2\pi} r f_n d\phi_s \quad (4)$$

where s, l, r, and ϕ_s represent surface area of integration, stack length of the machine (along the Z-direction), radius of the integrating contour, and angle component in cylindrical system of coordinates respectively.

Using equation (3)-(4), the electromagnetic torque can be calculated as shown by equation (5). These force distributions can be used to mitigate torque pulsation and the vibration in the stator frame either in design or in real time control stages.

$$T = \oint_S (\vec{r} \times \vec{f}_t).\vec{dS} \quad (5)$$

Fig.2 illustrates the distribution of the magnetic flux density in a 3-phase PMSM due to three phase excitation of the stator winding.

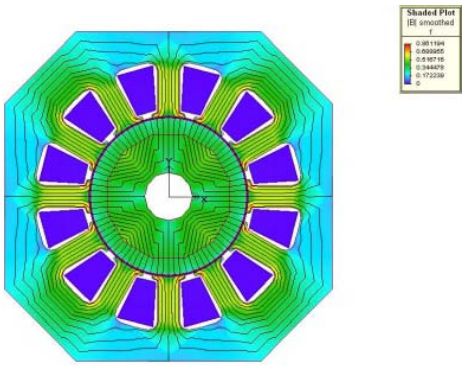

Fig.2 Distribution of magnetic flux density in a 3-phase PMSM

It is shown in Fig.2 that each conductor on the stator contributes to the tangential and radial components of the flux density in the airgap. Any change in the geometry within PMSM can alter the tangential and components of the flux density that are constituted by a conductor located at ϕ_{sk} as shown in equation (6).

$$B_{t,k} = B_t(i_k).h_t(\phi_s - \phi_{sk}) ; 0 \le \theta_r \le \frac{2\pi}{P} \;;$$

$$B_{n,k} = B_n(i_k).h_n(\phi_s - \phi_{sk}) \qquad (6)$$

where $P, B_t, B_n, h_t \; and \; h_n$ denote number of magnetic pole pairs, scaling function representing the dependency of the tangential and radial flux density upon the current magnitude, and impact of the geometry (one conductor) respectively. Also, ϕ_{sk} represents the location of the k^{th} conductor carrying a current of i_k.

The resultant tangential and radial components of the flux density in the airgap for any given rotor position can be expressed by using superposition (including the contributions from the permanent magnets) theory and a truncated generalized Fourier series as shown in equation (7) and (8). These expressions portray an elegant illustration of the separation between factors influenced by the structure of the machines($h_t \; and \; h_n$)and external excitation ($B_{t,k} \; and \; B_{n,k}$).

$$B_t(\phi_s, i_1, ..., i_m) = B_{t,pm} + \sum_{k=1}^{m} B_{t,k}(i_k).h_t(\phi_s - \phi_{sk}) \qquad (7)$$

$$B_n(\phi_s, i_1, ..., i_m) = B_{n,pm} + \sum_{k=1}^{m} B_{n,k}(i_k).h_n(\phi_s - \phi_{sk}) \qquad (8)$$

Equation (1) and (2) can therefore be rewritten by using the tangential and radial components of the force densities as follows:

$$f_t(\phi_s, i_1, ..., i_m) = \frac{1}{\mu_0}\left(B_t(\phi_s, i_1, ..., i_m).B_n(\phi_s, i_1, ..., i_m)\right) \qquad (9)$$

$$f_n(\phi_s, i_1, ..., i_m) = \frac{1}{2\mu_0}\left(B^2{}_n(\phi_s, i_1, ..., i_m) - B^2{}_t(\phi_s, i_1, ..., i_m)\right) \qquad (10)$$

In the same manner, equation (3) and (4) can also be rewritten to calculate the force density over the outer surface of a cylinder, which is located in the middle of the airgap, for each rotor position as shown in equation (11) and (12).

$$F_t(\theta_r) = P.L.R \int_0^{\frac{2\pi}{P}} f_t(.) d\phi_s \qquad (11)$$

$$F_n(\theta_r) = P.L.R \int_0^{\frac{2\pi}{P}} f_n(.) d\phi_s \qquad (12)$$

where $\theta_r, L, and \; R$ denote rotor position, stack length of the machines and radius of the integration surface respectively.

Seemingly, FRM contains key functions in equation (7) and (8), $h_t \; and \; h_n$ which are called as the basis functions. The basis functions have played a significant role in the formulation of the field reconstruction method. In equation (13) and (14), under unsaturated condition, FRM can calculate the distribution of field and force for at any given position due to stator currents when the pattern of excitation is known, and basis functions are identified. Also, the contributions of the permanent magnets will be adjusted for the new rotor position.

$$B_{t,k}(i_k) = B_t.i_k \qquad (13)$$

$$B_{n,k}(i_k) = B_n.i_k \qquad (14)$$

Equations (7) through (10) can identify the distribution of field/force for any given position. It must be noted that the contribution of the permanent magnets are captured separately using a series of FEA simulation. The basis functions h_t and h_n are related to an unsaturated slot-less and have characteristics as following:

- h_t has an even symmetry with respect to φ_s
- h_n has an odd symmetry with respect to φ_s.
- Periodic with respect to φ_s,

It should be noted that in the absence of stator excitation resultant tangential force forms an odd function resulting in zero average torque at every given point. Nevertheless, the radial forces exist even without any stator excitation. Fig.3 shows the tangential and normal components of the field density in the PM machine without stator excitation.

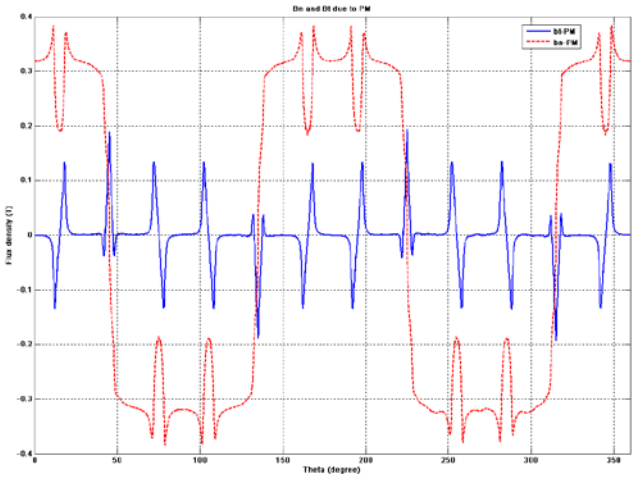

Fig. 3 Tangential and radial flux densities in airgap generated by permanent magnets

It can also be seen that radial component of flux density in a PMSM is primarily dominated by the field of the permanent magnet. Moreover, the normal component of force density yields a nonzero average and dominated by the normal component of the flux density even though it is without applying the stator current. Therefore, radial forces, which are

viewed as byproduct in electromechanical energy conversion process, are significantly larger than their tangential counterparts. It is also important to note that the tangential component of the flux density in the PMSM does not have a continuous profile and only appears at distinct positions where the stator/rotor coils are located. Integration of the tangential component of force density yields a zero average in the absence of excitation, which indicates that there is not motion when no excitation is applied.

From the above assumption, it must be noted that due to the periodic nature of the basis functions, they can be expanded by using a Fourier series, i.e.:

$$h_t(\varphi_s) = h_{0t} + \sum_{k=1}^{M} h_{kt} Sin(k\varphi_s) \quad (15)$$

$$h_n(\phi_s) = h_{0n} + \sum_{k=1}^{M} h_{kn} Cos(k\phi_s) \quad (16)$$

where M denotes the selected truncation point that would provide satisfactory precision. In the presence of saturation, the coefficients of the above series expansion depend upon current.

Fig.4 shows the algorithm of field reconstruction method for designs of the program and implement on microcontroller or digital signal processor.

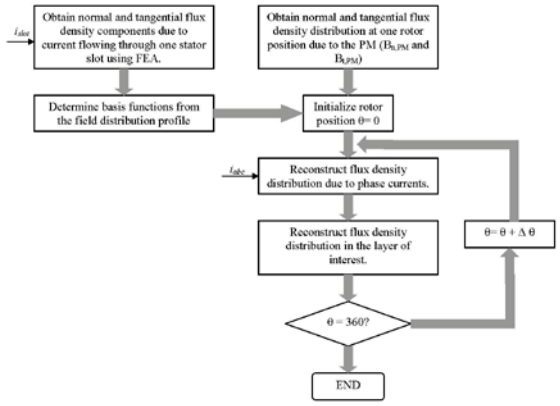

Fig.4 Flow chart of field reconstruction method (FRM)

III. EXPERIMENTAL SETUP

The experimental system may be divided into two main parts, which are PMSM (operating in generating mode) and the prime mover BLDC (operating in motoring mode) as seen in Fig.5.

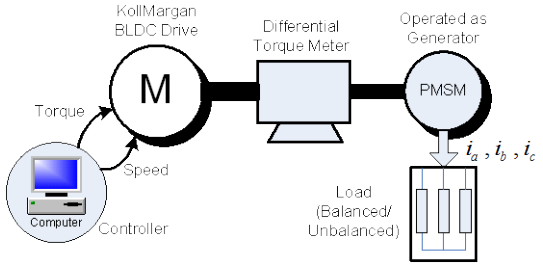

Fig. 5 Experimental setup

While the PMSM drive is running at a constant speed (as a generator)a set of balanced resistors were applied to its terminals. The stator phase currents are recorded. These three-phase currents are then injected into the FRM in Matlab/simulink in order to calculate the torque of PMSM. Consequently, the predicted torque of PMSM is compared with the torque of the prime mover (i.e. BLDC drive. The torque pulsation of PMSM is computed using the captured values in the inline torque transducer and with the knowledge of eth prime mover torque.

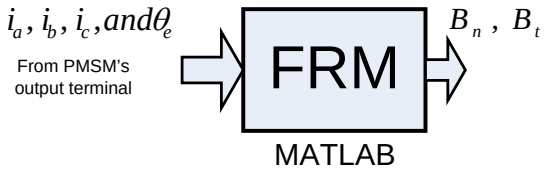

Fig.6 Demonstrating the calculation of FRM

IV. EXPERIMENTAL RESULTS

Fig. 7 shows the torque generated by between BLDC and PMSM. The PMSM's torque is the results of an electrical cycle of three-phase stator current. A balanced load was applied into the system and PMSM was operated at 334 rpm, and the FRM torque was computed from the 3-phase balanced current (top picture). The electromagnetic torque generated by the PMSM shows 12 pulsations which is in agreement with its geometry. Moreover, the results from BLDC (actual measurement)and PMSM (using FRM) are matched in terms of average torque and the period of torque pulsation.

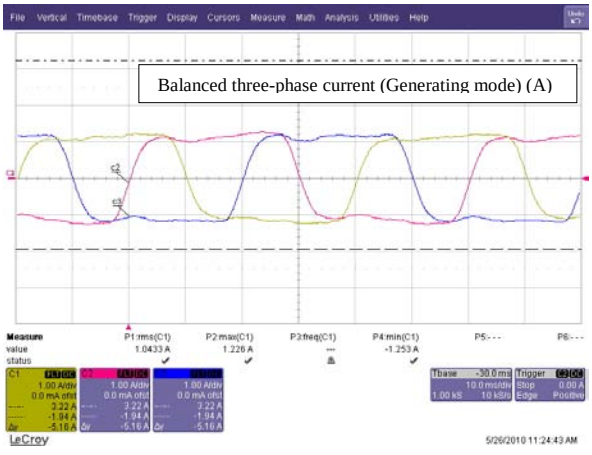

(a) Current waveforms at 334 r.p.m.

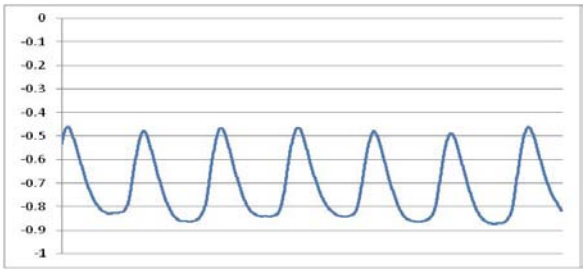

(b) Estimated torque using FRM technique

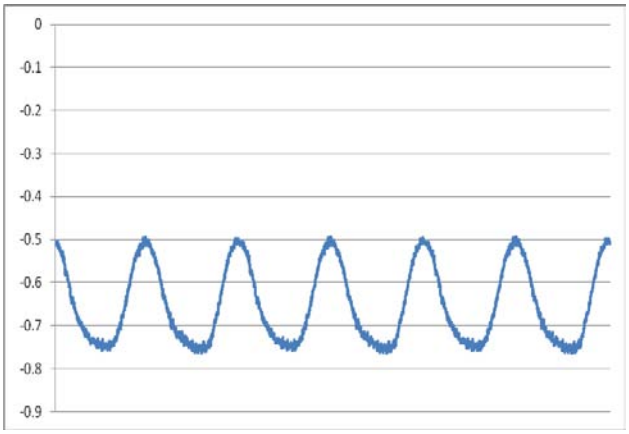

(c) Measured torque at 334 r.p.m.

Fig. 7 Electromagnetic torque under balanced load at 334 rpm

Fig. 8 shows an unbalanced three-phase current drawn from PMSM operating in generating mode, and at a speed of 1000 rpm. The measured current contain three electrical cycles. As a result, the torque pulsation will have 36 pulses due to the structure of PMSM (12 stator slots). Furthermore, the pattern of torque pulsation is a periodic function. The average torques from our proposed torque estimator and experimental data are in good agreement.

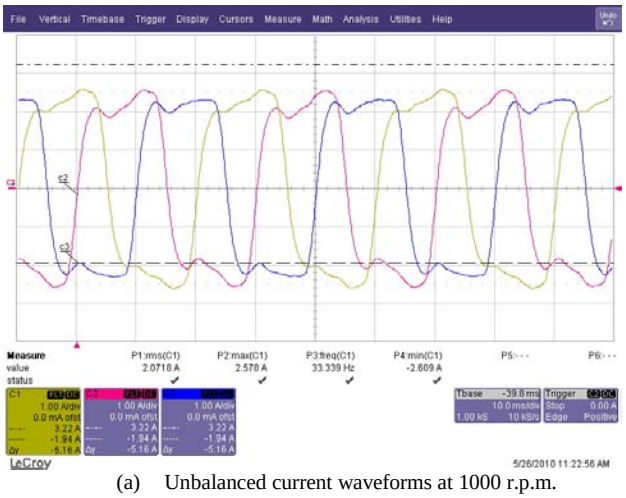

(a) Unbalanced current waveforms at 1000 r.p.m.

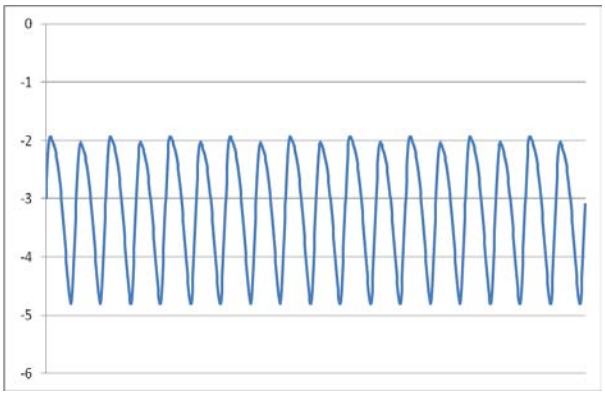

(b) Estimated torque using FRMAT 1000 r.p.m.

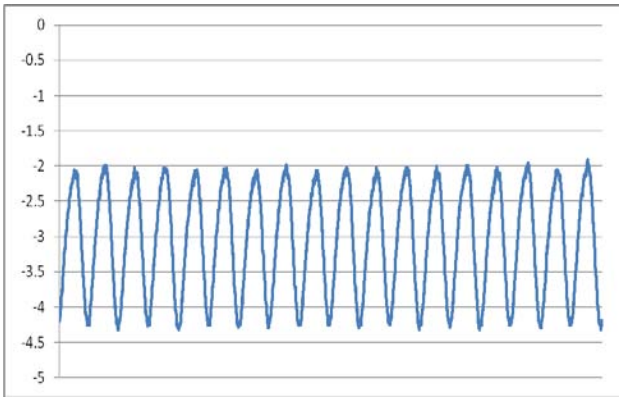

(c) Measured torque at 1000 r.p.m.

Fig. 8 Electromagnetic torque under unbalanced load at 1000 rpm

Once the accuracy of the torque estimator is established (as evidenced using the measured data here), one can use these values to effectively mitigate the effects of torque pulsation using a direct access to inexpensive torque data.

V. CONCLUSION

In this paper, a new torque estimator using field reconstruction method has been introduced. To accurately calculate torque pulsation, the tangential and normal components of magnetic field have been computed.

An experimental three phase PMSM has been used in this investigation. The investigation shows that FRM can accurately calculate the torque pulsation or cogging torque under balanced and unbalanced operations. As a result, FRM can be used in closed loop torque control scenarios thereby, eliminating the need for inline torquemeters. Furthermore, the FRM can be effectively used for optimal design practices.

REFERENCES

[1] D. C. Hanselman, "Effect of skew, pole count and slot count on brushless motor radial force, cogging torque and back EMF," *Inst. Elect. Eng. Proc.Elect. Power Appl*., vol. 144, no. 5, pp. 325–330, Sep. 1997.

[2] T. M. Jahns and W. L. Soong, "Pulsating torque minimization techniques for permanent magnet ac motor drives-a review," *IEEE Trans. on Ind. Electron*., vol. 43, no. 2, pp. 321–330, Apr. 1996.

[3] W. Zhu, B. Fahimi, S. Pekarek, "A field reconstruction method for optimal excitation of permanent magnet synchronous machines", *IEEE Trans. on Energy Conversion*, vol. 21, no.2, pp. 305 – 313, June 2006.

[4] A. Khoobroo, B. Fahimi, S. Pekarek, "A new field reconstruction method for permanent magnet synchronous machines", *IECON Int. Conf. on Ind. Electron.* pp. 2009 – 2013, Nov 2008.

[5] A. Belahcen, "Overview of the calculation methods for forces in magnetized iron cores of electrical machines," *presented at the Seminar on Modeling and Simulation of Multi-Technological Machine Systems*, vol. 29, pp. 4.1–4.7, Espoo, Finland, Nov. 1999.

[6] J. Y. Hung and Z. Ding, "Design of currents to reduce torque ripple in brushless permanent magnet motors", *Proc. Inst. Elect. Eng. B*, vol. 140, no. 4, pp. 260-266, 1993.

[7] F. Colamartino, C. Marchand, and A. Razek, "Torque ripple minimization in permanent magnet synchronous servo drive," *IEEE Transactions on Energy Conversion*, vol. 14, pp. 616–621, Sept. 1999.

[8] Q. Weizhe, S. K Panda, J. X. Xu, "Torque ripple minimization in PM synchronous motors using iterative learning control", *IEEE Transactions on Power Electronics*, Volume 19, Issue 2, March 2004, pp. 272 – 279.

[9] N. Matsui, T. Makino, and H. Satoh, "Auto-compensation of torque ripple of direct drive motor by torque observer", *IEEE Transactions on Industrial Applications*, vol. 29, pp. 187–194, Feb. 1993.